Chapter 2

Microstructural Evolution in Power Plant Steels

2.1 Power plant operation

In power plant, heat energy from fuel combustion or nuclear fission is used to produce jets of steam. The kinetic energy of the steam is converted to electrical energy by a system of turbines and a generator. Figure 2.1 shows the route followed by the steam and water. Water is pumped into the boiler and converted to steam, then superheated. It is injected through nozzles onto the blades of the high pressure (HP) turbines. Following this, it is reheated and sent to the intermediate pressure (IP) turbines and then to the low pressure (LP) turbines. The rotary motion of the turbines is used to drive the generator to produce electrical power, and the exhaust steam is condensed and recirculated.

The Carnot efficiency E of such a cycle is given by:

$$E = \frac{T_1 - T_2}{T_1} \tag{2.1}$$

where T_1 and T_2 are the absolute temperatures of the heat source and heat sink respectively. It is therefore desirable from both economic and environmental points of view to use as high an operating temperature as possible. Progress in power-plant alloy design has allowed T_1 to be increased from 370°C in the 1920s to a current level of 600°C or higher, and there is a drive

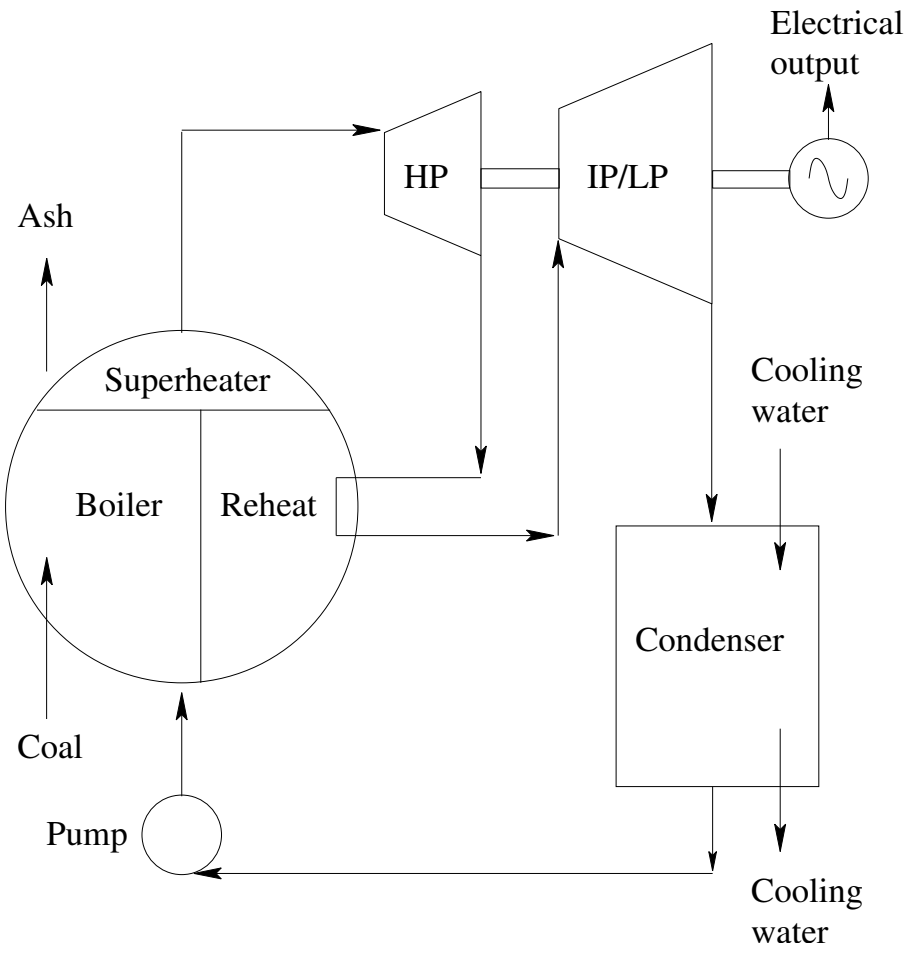

Figure 2.1: Schematic of a power plant steam cycle. After Cole, 2000.

towards further increases (Masuyama, 2001).

Steam turbines may be expected to withstand 28 or more years of continuous service (Berger *et al.*, 1993). These and many other components are exposed to conditions of 450–600°C and 15–100 MPa (Evans and Wilshire, 1985, Pickering, 1997).

Under such conditions, there are several life-limiting mechanisms, including corrosion, oxidation and fatigue, but one of the most important is creep, *i.e.* the progressive deformation of a component subjected to a high temperature and a stress which is lower than its yield strength. A typical tolerable creep strain rate for power plant is around 3×10^{-11} s^{-1}, which is equivalent

to 2% elongation over 30 years (Bhadeshia *et al.*, 1998).

Figure 2.2 shows a typical plot of strain against time in a sample subjected to a constant stress and a high temperature (Evans and Wilshire, 1993). The magnitude of the initial strain depends only on the stress. Usually the majority of the life is spent in the 'steady-state' regime, in which the strain rate is constant. The tertiary stage is characterised by an increase in creep rate, and ends with rupture.

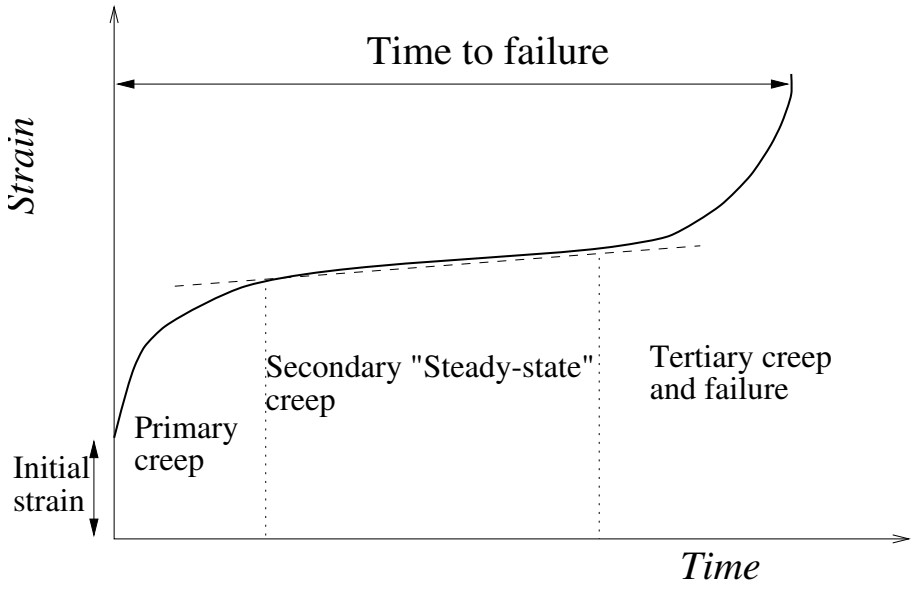

Figure 2.2: A typical strain-time curve showing the different regimes of creep (after Evans and Wilshire, 1993).

2.2 Creep mechanism

Creep only occurs to an appreciable extent when the temperature is above around $0.4T_M$, where T_M is the absolute melting temperature (Reed-Hill and Abbaschian, 1992). The predominant mechanism by which it occurs depends on temperature and stress. Deformation mechanism maps, in which the stress normalised against the shear modulus is plotted against the homologous temperature T/T_M, can be used to determine this (Frost and Ashby,

1982; Ashby and Jones, 1989). It is found that under typical power plant operating conditions, creep occurs by dislocation glide and climb, rather than by bulk diffusion.

Figure 2.3 shows how this occurs. The application of stress causes dislocations to move along slip planes until they encounter an obstacle, such as a second-phase particle. At room temperature, dislocations can only pass obstacles by cutting through them if they are coherent with the matrix, or by bowing out between them. However, at higher temperatures, the thermally activated diffusion of atoms to or away from the extra half-plane allows the dislocation to climb into a different, unobstructed slip plane, along which it can glide freely until it meets another obstacle and the process is repeated.

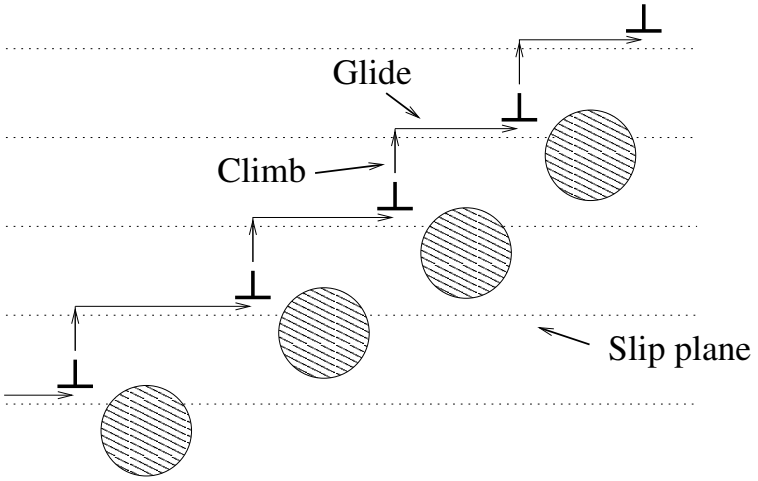

Figure 2.3: The processes of climb and glide.

2.3 Creep-resistant steels

Steels of the $2\frac{1}{4}$Cr1Mo type have been used in power plant for many decades, but recently 9–12Cr steels have been developed for use at higher operating temperatures. Both the compositions and the heat treatments of power-plant steels are chosen to give a fine, stable microstructure containing fine carbides. An austenitisation treatment to dissolve existing precipitates is

carried out above 1000°C, the exact temperature depending on the steel composition. The steel is then air-cooled. In $2\frac{1}{4}$Cr1Mo, this results in a predominantly bainitic microstructure, but 9–12 Cr steels are fully air-hardenable, and martensite is formed.

Tempering is then carried out, typically at around 700°C, to produce fine carbides and reduce the stored energy in the microstructure so that there is only a very small driving force for microstructural change during service. Bhadeshia *et al.* (1998) have calculated the stored energy of a power plant alloy in martensitic form is 1214 J mol^{-1} greater than that in its equilibrium state, whereas the post-tempering microstructure is only 63 J mol^{-1} above equilibrium.

Lower tempering temperatures give high creep rupture strength in the short term, but this decreases rapidly; tempering at a higher temperature gives better long-term creep properties (Yoshikawa *et al.*, 1986, Masuyama, 2001). This is believed to occur because the change from martensite to ferrite is complete after high-temperature tempering, but will occur during service if the tempering temperature is low.

2.3.1 Characteristics of martensitic steels

The transformation from austenite to martensite is diffusionless, occurring as a deformation of the parent lattice. On cooling sufficiently rapidly to suppress the diffusional ferrite and pearlite reactions and the intermediate bainite reaction, martensite formation begins at the martensite-start temperature M_s. The transformation is rapid and athermal. The M_f temperature marks the point at which transformation should be complete, but in practice, some retained austenite often remains. In plain carbon steels with <0.5 wt. % C, very little austenite is retained (2% or less) but higher carbon contents increase this proportion. Because the transformation from austenite is diffusionless, the martensite is supersaturated in carbon, and has a tetragonal crystal structure if the carbon content is sufficiently high.

2.3.2 Martensite morphology

Martensite forms in thin plates or laths on specific habit planes within the prior austenite grains. In order to accommodate the shape deformation of the transformation while maintaining a planar interface between the transformed and untransformed phases, the martensite slips or twins on a fine scale.

The dislocation density of ferrous martensites is of the order of 10^{11}–10^{12} cm^{-2}, similar to that achieved by severe cold work. In lower-carbon martensites (<0.5 wt. % C), only dislocations are usually present, but higher-carbon martensites also exhibit twinning, which is favoured by a higher yield stress.

Figure 2.4 illustrates schematically the structural levels in martensitic microstructures (Marder and Marder, 1969). The prior austenite grain boundary structure is preserved, and laths forming within the grains stop at these boundaries because the austenite grains do not, in general, have any special orientation relationship to one another. A packet is a region of laths with the same habit plane, and blocks are subunits of packets, in which the lath orientation is also the same. The combination of habit plane and orientation is known as a variant.

The sizes of both blocks and packets increased with increasing prior austenite grain size (Maki *et al.*, 1980). However, the clear block and packet structure in Figure 2.4 was only observed for carbon contents less than 0.5 wt. % in plain-carbon steels. Higher carbon contents gave a microstructure of irrationally arranged laths throughout the prior austenite grain.

In low-carbon martensitic steels (<0.5 wt. %C), the habit plane is $\{111\}_\gamma$, and the orientation relationship between the austenite γ and martensite α' is due to Kurdjumov and Sachs (1930):

$$\begin{array}{ccc} \{111\}_\gamma & \| & \{110\}'_\alpha \\ < 1\bar{1}0 >_\gamma & \| & < 1\bar{1}1 >'_\alpha \end{array} \tag{2.2}$$

Intermediate carbon contents give rise to a habit plane close to $\{225\}_\gamma$ and the same Kurdjumov-Sachs relationship, but in high-carbon martensites (>1.4 wt. %) the habit plane is close to $\{229\}_\gamma$ and the orientation relation changes to Nishiyama-Wasserman (Wassermann, 1933; Nishiyama, 1934):

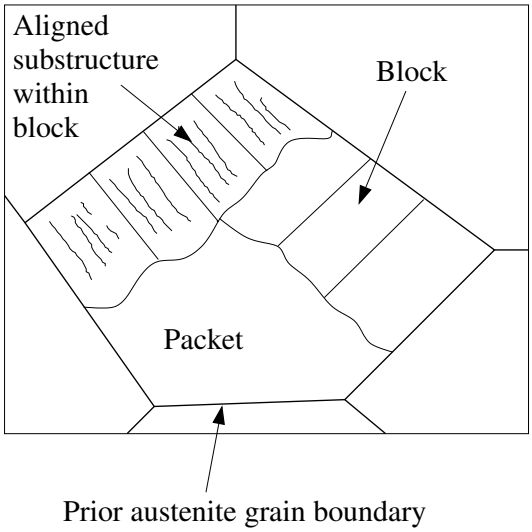

Figure 2.4: Levels of structure in martensite, (Marder and Marder, 1969).

$$\begin{array}{ccc} \{111\}_\gamma & \| & \{110\}'_\alpha \\ < 11\bar{2} >_\gamma & \| & < 1\bar{1}0 >'_\alpha \end{array} \tag{2.3}$$

2.3.3 Tempering of plain-carbon martensitic steels

The tempering of martensitic steels can be subdivided into four distinct stages (Balluffi *et al.*, 1951; Baker and Nutting, 1959: Honeycombe and Bhadeshia, 1995):

Stage 1: up to 250°C

Carbon in solution precipitates as laths or plates of ϵ-carbide, which has a definite orientation relationship with the matrix and is coherent with it in the early stages of precipitation. The tetragonality is reduced but not completely lost, and the matrix is still supersaturated in carbon.

Stage 2: 230–300°C

Retained austenite decomposes; it is believed to transform to bainitic ferrite and cementite.

Stage 3: 100–300°C

This overlaps with Stage 2. Cementite, Fe_3C, is precipitated as plates with a Widmanstätten distribution. It nucleates on ϵ-matrix interfaces or on twin, martensitic lath and prior austenite grain boundaries. The ϵ-carbides gradually dissolve as the cementite forms. Occurring concurrently with this is the loss of tetragonality of the martensite, which relaxes to ferrite as it loses its supersaturation.

Stage 4: 300–700°C (plain-carbon steels)

In plain-carbon steels, the final stage of tempering is the spheroidisation and coarsening of cementite particles. Coarsening begins between 300 and 400°C, but spheroidisation tends to occur at higher temperatures, up to 700°C. The driving force for these processes is the reduction in surface area, and hence in surface energy, of precipitates. Particles on lath boundaries or prior austenite grain boundaries are favoured for growth over those in the matrix since boundary sites allow easier diffusion and a source of vacancies to accommodate the less dense cementite. Recovery occurs between 300 and 600°C. Dislocations rearrange to form subgrains within the laths. Above 600°C, recrystallisation occurs, and equi-axed ferrite grains form at the expense of the original laths. Carbide particles retard grain growth by pinning grain boundaries, but eventually a microstructure of equi-axed grains and spheroidal carbides is produced. Further tempering causes a gradual coarsening of this structure.

Stage 4 in alloy steels

Chromium, molybdenum, vanadium, tungsten and titanium all form carbides which are thermodynamically more stable than cementite. Alloy carbide formation requires substitutional diffusion and therefore occurs more slowly than cementite precipitation, for which only interstitial carbon diffusion is necessary. Stages 1–3 occur in the same way as for a plain-carbon steel, and the cementite begins to grow, but it subsequently dissolves to be replaced by alloy carbide phases. Often, the new carbide is part of a precipitation

sequence of many phases, beginning with the most kinetically favoured and ending with the equilibrium phase. These changes may take place extremely slowly.

During the early stages of tempering, the precipitation of alloy carbides may increase the steel's strength above that of the as-quenched state (Figure 2.5). After this secondary hardening peak, the strength decreases monotonically with increasing tempering time.

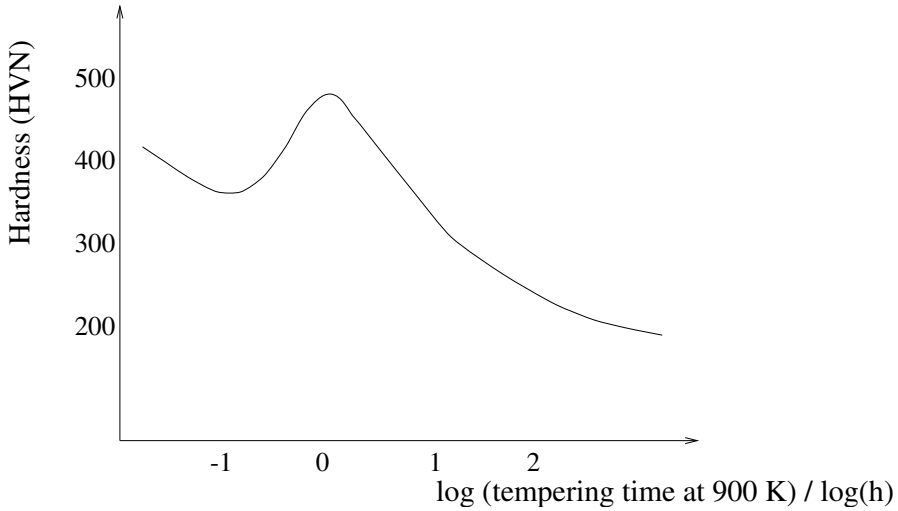

Figure 2.5: The secondary hardening effect in an alloy steel containing strong carbide formers (after Honeycombe and Bhadeshia, 1995).

2.3.4 Precipitation Sequences

The phases precipitating, and the order in which they form, depend on both the tempering temperature and the steel composition. Figure 2.6 maps the conditions for phase stability in $2\frac{1}{4}$Cr1Mo wt. % steel (Nutting, 1999). In alloy steels, carbides are described with a general formula M_xC_y or M_xX_y, where M signifies a metallic element and X a combination of carbon and nitrogen. In 9–12 wt. % Cr steels, precipitation sequences are similar, but occur at a much greater rate (*e.g.* Thomson, 1992).

Table 2.1 summarises the characteristics of precipitate phases found commonly in power-plant steels. Nucleation may occur in-situ, *i.e.* on the inter-

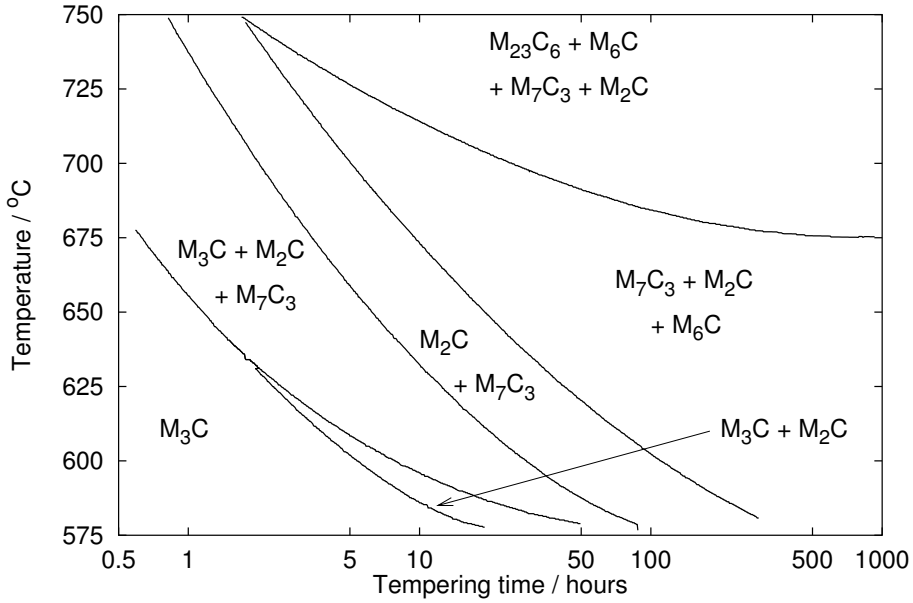

Figure 2.6: An updated version (1984) of the original Baker-Nutting carbide stability diagram (1959) for $2\frac{1}{4}$Cr1Mo steel, using new microanalytical techniques to identify phases (Nutting, 1999).

face between a pre-existing precipitate and the ferrite matrix. Alternatively, it may take place on intralath dislocations, lath boundaries, prior austenite grain boundaries or on the boundaries of subgrains formed during recovery of the dislocation structure. Such boundaries provide fast diffusion paths, enabling particles to coarsen more rapidly than they would if in the bulk.

M_3C

M_3C is the general formula for carbides with the same structure as cementite. Iron is in an approximately hexagonal close packed lattice, with distortions to accommodate the carbon atoms. The phase forms initially as Fe_3C, and then progressively enriches in substitutional solutes such as manganese and chromium (Woodhead and Quarrel, 1965). Its orientation relationship with the matrix is therefore the same as that of cementite. For example, Gingell *et al.* (1997) observed in 1Cr1Mo steels that M_3C occurred as elongated plates along $< 111 >_\alpha$.

Phase	Crystal structure	Nucleation site	Size	Shape	Benefits for creep?
M_3C	Orthorhombic	In-situ, MLB, PAGB	Coarse	Plates, then spheroidises	
M_2X	Hexagonal	D, MLB	Fine	Needle	Yes
M_7C_3	Trigonal	In-situ	Coarse	Spheroidal	No
$M_{23}C_6$	Cubic F	PAGB, MLB	Coarse	Spheroidal	No
M_6C	Cubic F	In-situ, PAGB, MLB	Coarse	Spheroidal	No
MX		Undissolved/ on MX	Fine	Spheroidal, platelike	Yes
Laves		PAGB, MLB, lath interior	Coarse	Spheroidal	Short-term?

Table 2.1: Data on common precipitates. D: dislocations, PAGB: prior austenite grain boundaries, MLB: martensitic lath boundaries. Crystal system data from Andrews *et al.*, 1967.

M_2X

The second phase to precipitate is commonly M_2X, which has a hexagonal structure (Andrews and Hughes, 1959). It commonly nucleates on dislocations and martensite lath boundaries (Raynor *et al.*, 1966), forming fine needles or rods. These have an orientation relationship with the matrix (Pitsch and Schrader, 1958):

$$\begin{array}{ccc} (0001)_{\mathrm{M}_X\mathrm{C}} & \| & (001)_\alpha \\ [11\bar{2}0]_{\mathrm{M}_2\mathrm{X}} & \| & [100]_\alpha \end{array} \tag{2.4}$$

It has also been seen growing perpendicular to austenite-ferrite interfaces (Edmonds and Honeycombe, 1973).

M_2X is very important to creep resistance in low-alloy steels, although it is only the carbides nucleating on dislocations which contribute significantly to this (Honeycombe and Bhadeshia, 1995). It dissolves rapidly in higher-chromium steels, but stabilising it in 12 wt. % Cr steel gave secondary hardening (Irvine *et al.*, 1960). However, the elements which favour its formation also promote the undesirable δ-ferrite phase.

$\mathbf{M_7C_3}$

M_7C_3 only appears if the chromium content is sufficiently high compared to that of other alloying elements (Woodhead and Quarrell, 1965). If molybdenum is present, $M_{23}C_6$ may form instead. If M_7C_3 is observed, it forms after M_2X (Baker and Nutting, 1959) or after M_3C without the intermediate M_2X stage (Janovec *et al.*, 1994). It nucleates close to cementite, possibly at the cementite-ferrite interface (Kuo, 1953; Baker and Nutting, 1959). Darbyshire and Barford (1966) state that the nucleation can be in-situ or on fresh sites.

This phase coarsens rapidly (Sakuma *et al.*, 1981; Yong Wey *et al.*, 1981) and is not thought to be beneficial for creep resistance.

$\mathbf{M_{23}C_6}$

This is rich in chromium (Woodhead and Quarrell, 1965) and is often an equilibrium phase in chromium-rich steels. It nucleates on prior austenite grain and martensite lath boundaries (Senior, 1989) and has also been identified adjacent to M_7C_3 (Nutting, 1999). It forms after either M_7C_3 or M_2X. The particles are large, and do not contribute to creep strength, but Bjärbo (1994) has suggested that it may retard microstructural coarsening by stabilising martensitic lath boundaries.

$\mathbf{M_6C}$

M_6C is an equilibrium phase in molybdenum-rich, relatively chromium-poor steels (Edmonds and Honeycombe, 1973; Tillman and Edmonds, 1974). It can nucleate on prior austenite grain boundaries and martensitic lath boundaries. Kurdzylowski and Zielinski (1984) report that it also nucleates in-situ on M_2X- or $M_{23}C_6$-ferrite interfaces, but Nutting (1999) has suggested that it instead forms by diffusion. Its rapid coarsening rate, greater than that of $M_{23}C_6$, make it a particularly undesirable phase (Vodárek and Strang, 1997), especially since it forms at the expense of finer carbides.

MX

These carbonitrides occur in complex 9–12 wt. % Cr alloys. They often have a NaCl-type cubic F structure (Woodhead and Quarrell, 1965). Fine, spheroidal MX particles, which are believed to remain in the microstructure during austenitisation, have been observed in the as-quenched steel (Janovec *et al.*, 1994). On tempering, these act as nucleation sites for platelike MX which forms in a 'V-wing' shape (Nickel *et al.*, 1995). MX is thought to be beneficial to creep properties because of its fine distribution and stability.

Laves phase

This intermetallic phase has the formula Fe_2M, where M represents molybdenum, tungsten or a combination of the two. It is an equilibrium phase in Mo- and W-containing 9–12 wt. % Cr steels. The favoured nucleation sites are initially prior austenite grain boundaries, then lath boundaries, and at the longest heating times, within laths (Senior, 1989). A review by Robson (1996) concludes that Laves phase is undesirable because of its coarseness and its depletion of the matrix in Mo and W. However, work by Hald (1995) suggests that Laves phase precipitation gives a greater strengthening effect than W in solution. According to Ishii *et al.* (1998), its presence at prior austenite grain and martensite lath boundaries contributes to creep strength. The coarsening rates of both W- and Mo-containing Fe_2M are high (Kubon *et al.*, 1997) so any strengthening effect does not last into the long term.

Other long-term phases

Three further phases have recently been identified in power plant steels. Z-phase was found in 12CrMoVNb steels (Strang and Vodárek, 1996). It is a complex nitride and appears to form at the expense of the fine precipitates of MX and M_2X which confer creep resistance; it is therefore undesirable. Mann *et al.* (1995) found rod-shaped M_5C_2 in post-service $1Cr\frac{1}{2}Mo$ steels. This appeared to nucleate on M_2X. The intermetallic μ-phase (Fe_7W_6) is believed to improve high temperature creep strength (Igarashi and Sawaragi, 1997).

Figure 2.7 shows a typical tempered martensitic microstructure in 9–12 wt. % steel.

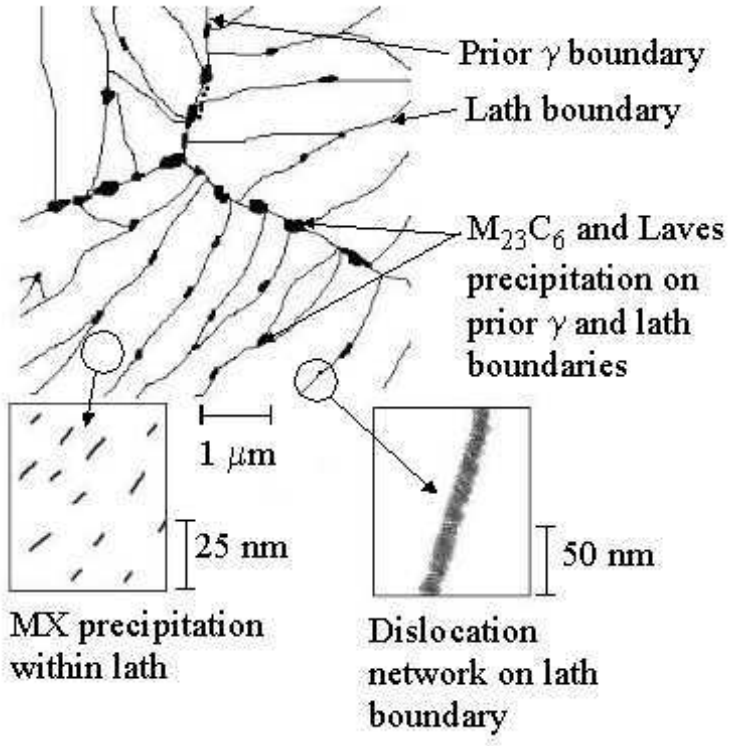

Figure 2.7: Typical microstructure of tempered martensitic 9–12 wt. % steel (after Masuyama, 2001).

2.4 Differences in bainitic microstructures

Bainite can occur in two forms (Honeycombe and Bhadeshia, 1995). 'Upper bainite' forms at a higher temperature (550-400°C) and consists of fine ferrite plates of length approximately 10 μm and thickness approximately 0.2 μm, growing in clusters (sheaves) in which all the plates are parallel and of the same crystallographic orientation, and separated by low-misorientation grain boundaries or by cementite precipitates. Lower bainite, which forms between 400 and 250°C, contains cementite precipitates within ferrite plates as well as between them.

Bainite is closer to equilibrium than martensite, being only slightly supersaturated in carbon. Cementite particles are already present and these tend to be larger than the cementite formed on tempering of martensite. The dislocation content is also smaller than that of martensite. In plain-carbon bainite, short-term tempering gives little change in microstructure, but a significant drop in strength is seen when the plate-like ferrite and cementite spheroidise to an equiaxed structure. The effect of alloying with carbide-forming elements is the same as for tempered martensite, but alloy carbides form on a longer timescale.

Baker and Nutting (1959) investigated the effect on tempering kinetics of using a martensitic rather than bainitic starting microstructure in $2\frac{1}{4}$Cr1Mo steel. Differences were observed, but they were very small, because the defect densities of the two starting microstructures were very similar. Bhadeshia (2000) raised the question of why the higher-Cr steel was martensitic, and concluded that this was a by-product of alloying to increase oxidation and corrosion resistance. However, he suggested that the fine plate-like microstructure in martensite may contribute to creep resistance by impeding dislocation motion. Yamada *et al.* (2002) found that in 9Cr3W3Co steels, water-quenching instead of air-cooling gave longer creep rupture lives. Quenching gave a better distribution of MX particles, suppressing complex MX phases and accelerating the formation of more beneficial VC.

2.5 Changes during service

In $2\frac{1}{4}$Cr1Mo steels, M_2X provides long-term creep resistance, but this phase dissolves rapidly when the chromium content is higher. A review of strengthening mechanisms in tempered high-Cr creep resistant steels by Maruyama *et al.* (2001) concludes that dislocations, solutes, intragranular particles (MX) and particles on boundaries all contribute to creep strength, but not in a simple additive manner.

During creep deformation, the dislocation substructure of the tempered steel, which is stable with respect to temperatures up to 650°C in the absence of stress, undergoes recovery into a subgrain structure (Nickel, 1995;

Iwanaga *et al.*, 1998; Cerjak *et al.*, 2000). The growth of these subgrains is accompanied by a reduction in dislocation density, and reduces the creep resistance.

2.5.1 Lath coarsening, recovery and recrystallisation

Martensite laths in 9Cr-W steels subjected to creep were found to coarsen concurrently with $M_{23}C_6$ particles (Abe, 1999). An increase in the tungsten content retarded the coarsening of both the $M_{23}C_6$ and the laths, while causing the precipitation of Laves phase. It was concluded from this that $M_{23}C_6$ particles are more effective than Laves phase for pinning lath boundaries. The lath coarsening observed by Abe occurred by lath boundary triple point migration (Figure 2.8).

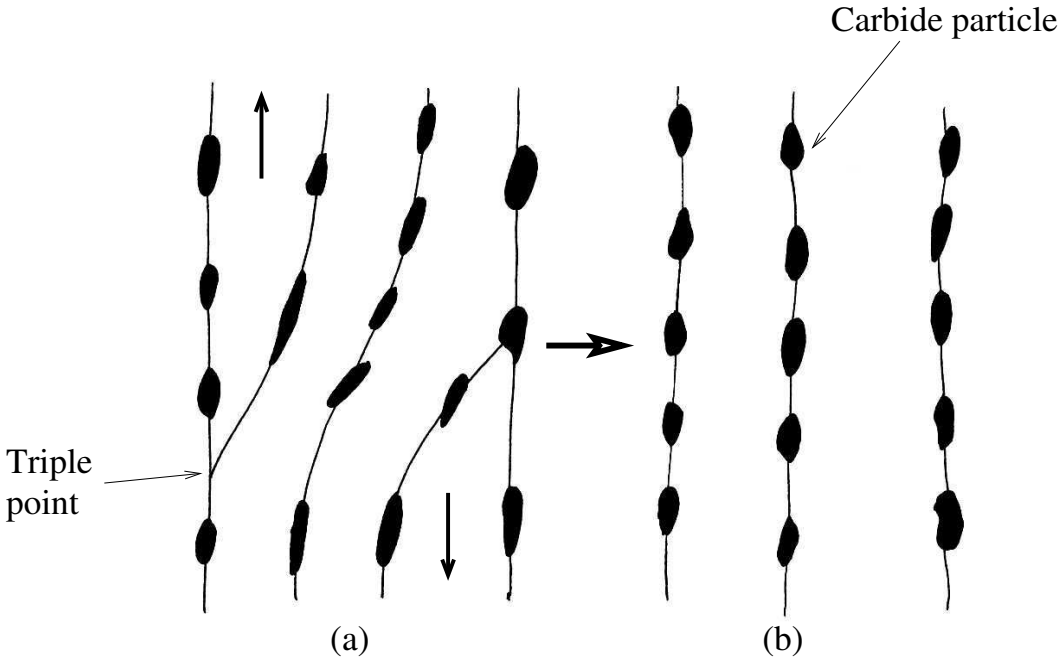

Figure 2.8: Lath coalescence: Triple points migrate and lath boundaries coalesce (a) to give a coarser structure (b). After Abe, 1999.

2.5.2 Cavitation and final failure

Creep rupture may occur in a more brittle or more ductile manner; cavities occur at smaller strains when the ductility is low (Beech *et al.*, 1984). Second-phase particles on grain boundaries can act as nucleation sites for voids (Martin, 1980). Grain boundary triple points also concentrate stress during grain boundary sliding in creep, resulting in cavitation (Watanabe, 1983).

In power-plant steels, failure can be promoted by preferential recovery at prior austenite grain boundaries (Kushima *et al.*, 1999; Abe, 2000). The large, rapidly coarsening particles on grain boundaries deplete the local matrix of solutes and fine particles, and the resulting recovered region acts as a strain concentrator and is able to crack easily.

2.6 Design life and remanent life estimation

Conservative component design lives are used to accommodate the effects of microstructural heterogeneity and variation in service conditions. The working stress is set at around 0.8 times the value of the lower bound of creep rupture stress at the intended life (Halmshaw, 1991). It has often been found that components reaching the end of their design lives are still in a safe condition for several more years of use. Bhadeshia *et al.* (1998) have reviewed the techniques available for the estimation of the remanent lives of such components. These subdivide into methods based on mechanical properties such as hardness and impact toughness, those involving microstructural observation, and those in which other properties, such as resistivity or density, are measured and used to infer the component condition. However, Bhadeshia *et al.* concluded that none of these techniques gave a sufficiently comprehensive characterisation to be used in isolation. Also, implementation often requires a plant shutdown, the expense of which contributes a great deal to the cost of life extension as opposed to component replacement at the end of the design life.

2.7 Scope for magnetic methods

It is clear that there is a need for additional microstructural monitoring techniques, especially those which can be used in-situ with minimal preparation, and which give a comprehensive characterisation of the component state.

Ferritic power plant steels are ferromagnetic, allowing the use of magnetic monitoring methods. Magnetic techniques are routinely in use for crack detection in ferromagnetic components, and appear promising for the measurement of stress effects. For example, a programme for the evaluation of structural materials in nuclear power plant after tensile and fatigue loading, which includes the measurement of several magnetic properties, is under development in Japan (Uesaka *et al.*, 2001).

The aim of this study is to investigate their usefulness as a method of microstructural evaluation for the purpose of remanent life estimation in power plant steels. This requires an understanding of the relationships between magnetic properties and the characteristics of microstructural features such as grain boundaries and carbides. Chapter 3 and Chapter 4 discuss the progress made so far in understanding these.